Proceedings of the Project Review, Geo-Mathematical Imaging Group (Purdue University, West Lafayette IN), Vol. 1 (2010) pp. 221-232.

PARTICLE SWARMS IN SMOOTH-WALLED FRACTURES

LAURA J. PYRAK-NOLTE* AND MICHAEL K. OLANDER†

Abstract. Numerical simulations and experimental measurements were performed to determine the effect of smooth-walled fractures on particle swarms. The numerical simulations were based on a particle interaction approach that included a first order approximation for particle-wall interactions. Transparent cubic samples (100 mm x 100 mm x 100 mm) containing synthetic fractures, with uniform aperture distributions, were used to quantify the effect of aperture on swarm formation, swarm velocity, and swarm geometry using optical imaging. A series of experiments were performed to determine how swarm movement and geometry are affected as the walls of the fracture are brought closer together from 50 mm to 1 mm. The simulations and experimental data confirm that swarm velocity decreases with decreasing aperture because of a significant increase in drag on the particles from the walls. However, the experiments showed that by increasing the swarm particle number density, the swarm cohesiveness and velocity were maintained over longer distances in the fracture.

1. Introduction. For any subsurface infrastructure or fluid production/sequestration project, knowledge of the rock and fluid properties at the site is required, as well as an understanding of the physical, chemical, and biological processes that act on these materials. There is a strong desire in the scientific and petroleum community [1] to develop nano- and/or micro- sensors that can be transported and distributed into a subsurface formation and that report back information on rock structure & lithology, porosity, pore connectivity, fluid chemistry, fluid viscosity, biological activity, temperature, pressures, etc. Distributed subsurface sensor networks have the potential to overcome the limited spatial resolution and imaging capability of most geophysical methods. Thus, the idea of creating distributed subsurface sensor networks is attractive to provide information on length and time scales not possible with current state-of-the-art geophysical methods. The ability to extract or sequester fluids and materials in the subsurface requires detailed information on the mechanical, hydraulic and chemical integrity of subsurface formations. Current geophysical methods can provide either detailed information in a small volume adjacent to a borehole, or information over larger volumes, but at much lower spatial resolution. To bridge this gap, nano- and/or micro- sensors could be distributed to target locations in the subsurface to provide local detailed information of the formation, fluids, and microbial life.

Nano- and micro-sensors for subsurface applications may take the form of environmentally sensitive sensors that are flowed through a system and then optically interrogated as they exit the system at an outlet, or RF (radio frequency wireless) sensors that are distributed throughout a region of interest and their response to subsurface conditions are interrogated in place. Environmentally sensitive nano-sensor technology has progressed rapidly in recent years, making them available to sense their local environments for temperature, pH, electrolyte concentration, electric field, magnetic field, and molecular sensors that target specific biomolecules or toxins [2-8]. Developing in parallel, but largely independently, has been the wireless revolution, as wireless device sizes and costs have continually shrunk. The small size and low cost has motivated the concept of distributed RF sensor networks that can be used for broad-area sensing and surveillance.

Given the scale of subsurface reservoirs (kilometers), there are challenges related to the readout of these sensors in the subsurface because rocks and conductive fluids attenuate RF signals. These challenges are potentially met by the use of collaborative sensors or sensor swarms. Collaborative sensors are either ensembles of many individual sensors that are maintained and collectively readout, or a semi-coherent ensemble that is maintained between boreholes for optical interrogation at the well. A RF sensor swarm would consist of a number of RF sensors that combine their signals coherently, enabling a wide field of sensors to be interrogated, whereas single sensors would be below the detection limit. A swarm of environmentally-sensitive functional nano-sensors would maintain a semi-coherent group so that as many sensors reach the exit borehole as possible, given

*Department of Physics, Purdue University, West Lafayette, IN 47907, Department of Earth and Atmospheric Sciences, Purdue University, West Lafayette, IN 47907

†Department of Physics, Purdue University, West Lafayette, IN 47907

the potential for sensor loss over large distances due to pore straining, chemical immobilization, etc.

Sensors that are distributed by flowing them through a fracture network between boreholes will be affected by the geometry of the fracture network, by the sensor morphology (size & shape), by the surface features of the particles (smooth versus rough), by the spatial distribution of the particles within the fracture plane, and fluid/rock/sensor chemistry. From the literature [7-13], current biomedical nano-sensor technology and other RF sensors span a wide range of physical properties and morphology in terms of size and shape. The ability to create swarms of nano-/micro- sensors from a particular sensor morphology in a fracture network is unknown. A challenge is to determine how to create, maintain, and control sensors swarms to deploy the sensors to targeted locations within a fracture network.

In this paper, we take the initial step of understanding the behavior of a swarm of particles in constrained geometries, i.e., within smooth-walled fractures. A swarm is group of particles that exhibits collective behavior and remains a cohesive entity over long periods of time. A swarm is a dilute suspension of particles with density that only differs slightly from the density of the background fluid. The process by which a swarm forms depends on interparticle interactions and particle-wall interactions, particle size, number of particles, particle concentration, shape of the particles, and fluid velocities. The underlying forces are gravitational, buoyancy, and drag, while particle-particle and particle-wall interactions also include double layer repulsion or attraction, Van der Waals attraction, and short-range forces such as hydration and steric repulsion [15]. Buoyancy and drag forces depend on the shape/size of the particle.

For dilute suspensions (0.4% - 1.0% by weight) and low Reynolds numbers (0.023 0.283), Adachi et al. [14] showed numerically and experimentally that the formation of a swarm was robust against the viscosity and density of the fluids and the particle size. Swarm formation in their experiments was determined by the settling velocity of a single particle relative to the falling velocity of the swarm. The settling velocity, vsettling, of a spherical particle is given by

$$v_{settling} = \frac{(\rho_p - \rho_f) g d_p^2}{18 \mu_f} \tag{1.1}$$

where ρ_p and ρ_f are the densities of the particle and the fluid respectively, g is the gravitational acceleration, d_p is the diameter of the particle and μ_f is the viscosity of the fluid. The mean falling velocity of the swarm, v_{swarm}, is given by

$$v_{swarm} = \frac{4}{3} \frac{gD^2}{C_d\, Re} \frac{\rho_s - \rho_f}{\mu_f} \left[1 + \left(\frac{1}{C} - 1 \right) \frac{\rho_s}{\rho_f} \right]^{-1} \propto CD^2 \tag{1.2}$$

where C is the weight concentration of particles, Re is the Reynolds number of the swarm ($Re = Dv_{swarm}\rho_f/\mu_f$), D is the swarm diameter, and C_d is the coefficient of drag of the swarm. When the concentration is low and $C_d\, Re$ is taken to be constant, vswarm is proportional to CD^2. Equations (1.1 & 1.2) apply to a mono-dispersion of spherical beads of equal size and equal weight [14] The dilute concentration assumption minimizes hydrodynamic interactions among particles. Adachi et al [14] found experimentally that a swarm of particles forms when the falling velocity of the swarm of particles is more than 16 times larger than the settling velocity of an individual particle. Roughly, the length scale that controls swarming is the particle spacing. Nitsche & Batchelor [16] noted that the falling of a particle swarm through a liquid is similar to the falling of a heavy fluid through a lighter fluid, except that the particle swarm has the additional feature that the particles fall relative to the fluid they are immersed in, i.e. the particles within the swarm fall and circulate within the drop.

Other studies have examined theoretically, computationally, and experimentally the formation of swarms [17-21] leading to modified forms of equations (1.1 & 1.2) that use discrete particle approaches versus continuum methods to examine swarm formation. As Machu et al [17] & Metzger et al. [18] have shown, swarms evolve and can disintegrate over time. Swarm break-up occurs as particles leak-off the swarm, and the rate of leakage varies depending on the swarm shape [18]. All

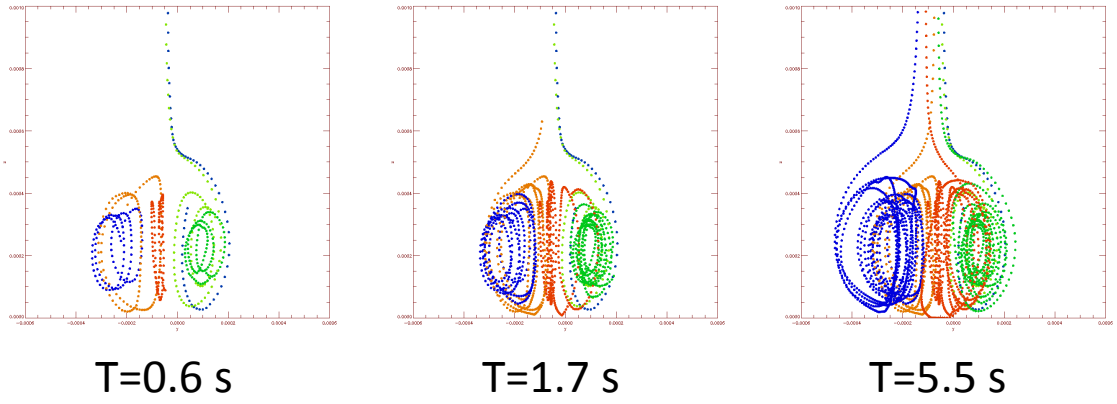

FIG. 1. *Time-lapse graphs of the particle motion of five particles (represented by different colors) for swarm composed of 400 particles. The motion is in the frame of the swarms.*

of these studies have examined the formation and evolution of swarms [17-21] in quiescent fluids in beakers, water-cylinders, water-tanks, etc., but never in the constrained geometries of fractures.

Building on the swarm community research, we have performed numerical and physical experiments to create and study the time evolution of swarms in smooth-walled fractures.

2. Experimental Set-up. Transparent cubic samples containing synthetic fractures, with uniform aperture distributions, were used to quantify the effect of aperture on swarm formation, swarm velocity, and swarm geometry using direct optical imaging. A smooth-walled fracture was created from two polished acrylic rectangular prisms, each measuring 100mm x 100mm by 50 mm. A series of experiments were performed to determine how swarm movement and geometry are affected as the aperture of a fracture is reduced from 50 mm to 1 mm. During the experiments, the fracture was fully saturated with water. We created the swarms using two different particle sizes in dilute suspension ($\sim$ 1.0% by mass). The particles were 3 micron diameter fluorescent polymer beads and 25 micron diameter soda-lime glass beads. The fluorescent beads have an excitation peak at 542 nm and emission peak at 612 nm. A red filter (no. 25) was used to image the fluorescent beads that fluoresce in the red. Each swarm was formed by dropping a 15 μl mixture of beads and water ($\sim$1 solids by mass). A programmable syringe pump was used to form a drop of bead-water solution. The syringe was a standard BD 10mL with an inner diameter of 0.260 mm and an outer diameter of 0.514 mm. The pump was set to release 15 μl volume. An infuse-refill method was used to reduce particle streaming after the formation and release of the drop. The swarms composed of 25 m beads where dropped from a height of 13 mm above the waters surface. The 3 μm particle swarms could not be dropped above the surface because the integrity of the initial swarm drop could not be maintained, i.e., the drop of particles and fluid would break up on impact and the beads would float on the surface. The 3 μm particle swarms were released 13 mm below the surface of the water.

The swarm behavior was imaged using an optical fluorescent imaging system composed of a CCD camera and illuminated by a 100 mW diode-pumped doubled YAG laser. The CCD camera captured images perpendicular to the fracture plane at a rate of 4 fps to 18 fps depending on the light intensity, binning and size of the region of interest. The pixel edge length in an image was approximately 125 μm. The resolution was sufficient to image the swarm behavior but not individual particles.

3. Simulation Approach. Swarm evolution was simulated using a particle interaction approach based on Nitsche & Batchelor [16]. In this approach, particle-particle interactions are modeled using a Stokeslet approach. Particle-wall interactions, F_i, are included by using the first order term in the Faxen [22] approximation. The following equations are used to determine particle

velocity, V_i for each particle in the swarm

$$V_i = \frac{1}{6\pi\mu a}\left[-K + U_i + F_i\right]$$
$$U_i = T 6\pi\mu a\left[-K + F_i\right]$$
$$T = \frac{1}{8\pi\mu r}\left[I + \frac{r \otimes r}{r^2}\right]$$
$$F_i = 6\pi\mu a\left(\frac{9a}{8d}U_{xj},\ \frac{9a}{16d}U_{yj},\ \frac{9a}{16d}U_{zj}\right)^T$$

where

- K represents the component from gravity and is equal to $\Delta mg = (m_{particle} - m_{fluid})g$.
- U_i is the ambient fluid velocity caused by the motion of the other particles
- F_i is the force on the wall by particle 1
- F_j is the force from the wall on particle j
- T is the Stokeslet tensor
- r is the position vector for each particle
- a is the particle radius and μ is the fluid viscosity
- d is the distance from the wall

One equation was used for each particle in the swarm. A Runge-Kutta approach was used to solve the system of equations to determine the position of each particle in the swarm for an initial spherical swarm shape composed of 25 micron particles distributed randomly within a spherical volume with a diameter of approximately 0.485 mm. The number of particles used in the simulations of smooth-walled fractures was 400. Simulations with 1000 particles were used to examine the effect of particle density on swarm stability. A time step of 0.005 s was used in the simulations. The effect of particle-wall interactions was studied for a smooth-walled fracture with constant aperture. Simulations were run for apertures of 0.5 mm, 1 mm, 2mm, 4 mm, 8 mm, 16 mm, 32 mm, 64 mm and for no walls.

4. Results & Discussion.

4.1. Particle Interactions and Particle Density. Using swarms to transport groups of particles through a fracture requires maintaining a cohesive body of particles together as long as possible. Several researchers have studied swarm evolution as a function of time in unconfined fluids, i.e., no walls [16-18]. We simulated swarm formation in unconfined (no walls) fluid to establish the basic behavior of swarms and included the effect of particle-wall interactions.

Figure 1 gives an illustration of the particle motion within the swarm as it falls under gravity. In Figure 1, the particle motion is shown in the frame of the swarm for elapsed time for five particles. Once the swarm is released and falls under gravity, there is a high pressure under the center of the swarm that causes the fluid external to the swarm to flow past the swarm. This pressure field results in internal pressure fields within the swarm that cause the particles to circulate in a manner similar to flow circulation within a heavy drop (with no particles) relative to a lighter fluid [14,16].

In the experiments, the number of particles that compose our swarm are roughly 7200 particles (for the 25 micron diameter beads) and 107 (for the 3 micron diameter beads). Running simulations with that number of particles is computationally expensive. Thus, the first simulations that we analyzed examine the effect of particle density on swarm velocity using 400 and 1000 particle swarms with the same swarm diameter (0.5 mm). Figure 2 compares the evolution of these two swarms. Increasing the number of particles within the swarm increases the density contrast between the swarm and surrounding fluid. As expected, the denser swarm falls initially with a swarm velocity that is larger than the low density swarm velocity by a factor of 2.5. This factor is the ratio of particle numbers of the two swarms ($\sim$1000/400). The magnitude of the initial swarm velocity is also consistent with the approximation given by Nitsche & Batchelor [14] of $V_{swarm}/V_{particle} \sim 1 + (6N * a/5R)$ where N is the number of particles, and a & R are the radii of the particle and

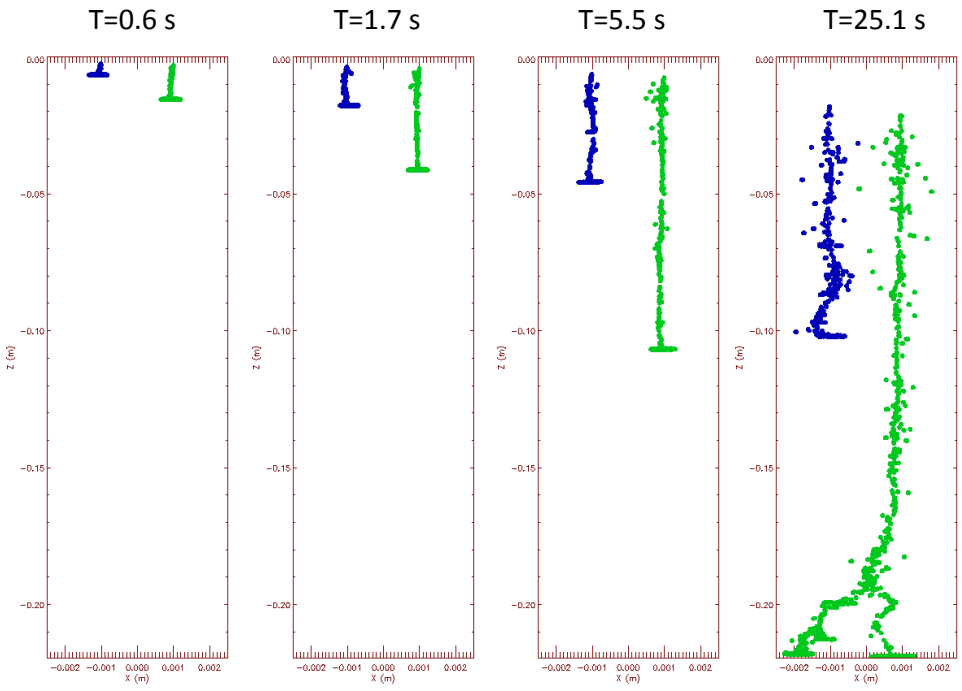

FIG. 2. *Time-lapse graphs of the N=400 (blue on left) and N=1000 (green on right) particle swarms showing that the high particle density swarms falls faster. The dense swarm bifurcated as it fell under gravity.*

the swarm, respectively. For a particle diameter of 25 microns and a swarm diameter of 0.5 mm, the velocities obtained with this approximation are 13.6 mm/s and 33.2 mm/s for N=400 and 1000 particles, respectively. As seen in Figure 3, our simulations result in slightly lower values of initial swarm velocity (11.6 mm/s & 26.4 mm/s). The settling velocity for both swarms from the simulation asymptote to 1.77 mm/s (N=400) and 2.0 mm/s (N=1000), with the low density swarm approaching the asymptote at earlier times. For comparison, the settling velocity for a single 25 micron particle in water is 0.54 mm/s based on equation 1.1.

4.2. Particle-Fracture Interactions. Faxen [22] derived an anlytical expression for the effect of walls on a single falling sphere and a method of reflection approach was used by Brenner [23] for a sphere moving towards a plane wall. Graselli & Lobry [24] showed from experiments and simulations that this analytic form can be used to first order approximation without significant error. We incorporated the effect of a smooth-planar fracture of constant aperture in the simulation as described by the F_i & F_j terms given in the Simulation Approach section. The expressions for F essentially increase the drag on the particle for motion parallel or perpendicular to the walls.

Figure 4 shows the results of the effect of aperture on the shape of the swarm and distance that the swarm fell in 20.1 seconds. Before release, each swarm has the same number of particles (N = 400) and same random positions within a spherical volume with a diameter of ~ 0.495 mm. When the aperture is comparable to the swarm radius (dark blue swarm in Figure 4), the drag in the vertical direction is significant and most of the particle-particle and particle-wall interaction results in a horizontal spreading of the swarm along the fracture. As the aperture of the fracture increases, the swarm falls to greater depths within the first 20.1 seconds. However, the stability of the swarm varies. For fracture apertures of 8 mm, 16 mm and 32 mm, the swarm breaks up and bifurcates into multiple branches at shallow depths. The swarm in the 64 mm aperture was found to bifurcate after 25 seconds and at a deeper depth along the fracture.

From simulations, Metzger et al. [18] found that the probability of a swarm breaking up or

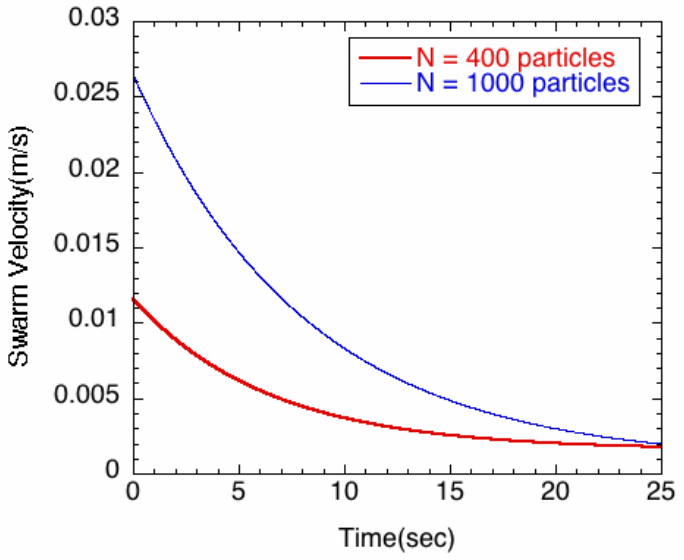

FIG. 3. *Swarm velocity as a function of time for the two swarms shown in Figure 2.*

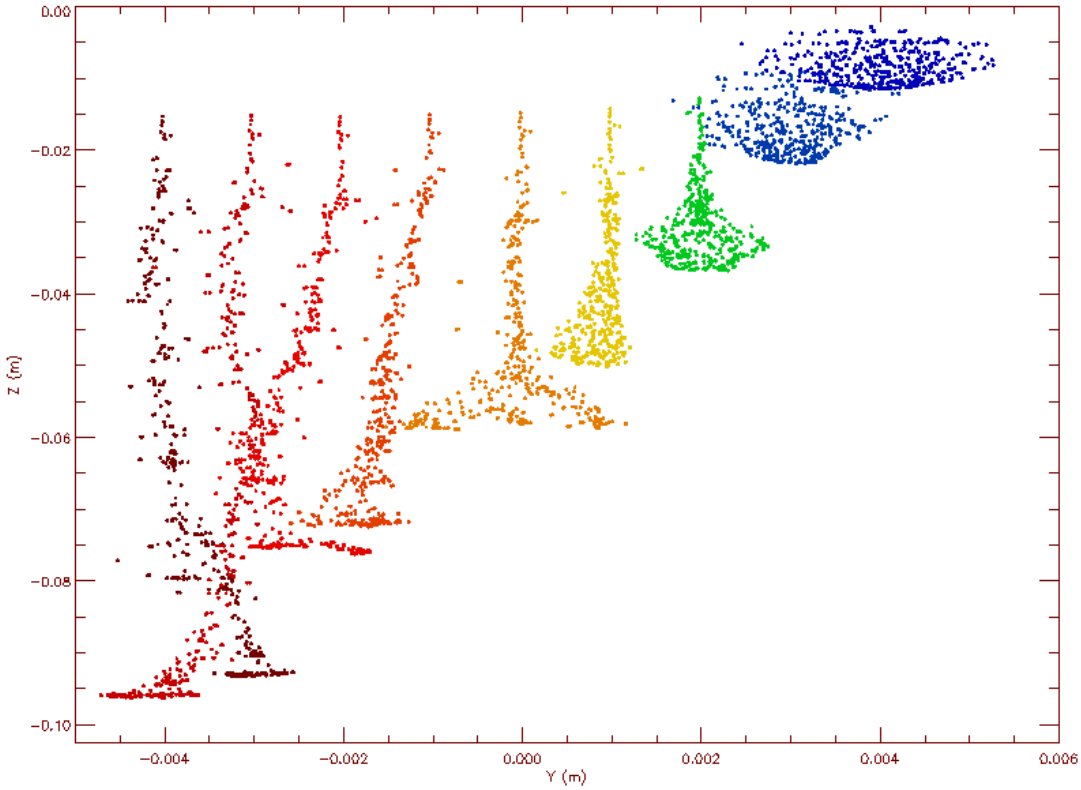

FIG. 4. *Simulation results for nine swarms released in a smooth-walled fracture with a constant aperture of 0.5 mm, 1 mm, 2mm, 4 mm, 8 mm, 16 mm, 32 mm,64 mm and for no walls (from right (dark blue) to left (dark red) in the graph).*

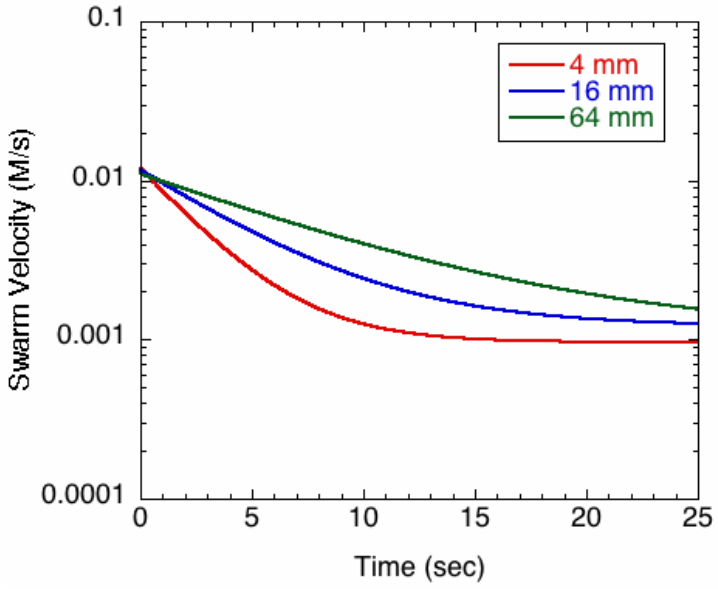

FIG. 5. *Comparison of swarm velocity for a swarm released in a fracture with uniform apertures of 4 mm, 16 mm and 64 mm (same swarms as in Figure 4.)*

destabilizing was low for swarms with particle numbers N $\leq$ 500, but swarms with N $\geq$1000 the probability of breakup was 1. From our simulations, we observed that particle interactions with a smooth wall fracture tend to lead to bifurcations.

The swarm velocity as a function of time is shown in Figure 5 for fractures with uniform apertures of 4 mm, 16 mm and 32 mm. The initial velocities of these swarms are approximately the same ($\sim$ 12 mm/s) but asymptote to slightly different settling velocities (0.96 mm/s, 1.3 m/s and 1.6 m/s for 4mm, 16 mm and 64 mm, respectively). Smaller fracture aperture causes quicker relaxation of the swarm to its settling velocity. Though the walls for the 64 mm aperture fracture are quite far apart, and any one individual particle experiences only a small force from the walls, the sum of the forces from the wall on all 400 particles results in swarm behavior that deviates from the case with no walls.

5. Experiments. The simulations showed that the swarm settling velocity decreases with decreasing fracture aperture and that the swarms spread out laterally in small aperture fractures. From laboratory measurements, we confirm that small-aperture fractures cause the swarms to fall to a shallower depth, to spread out laterally (Figure 6), and to asymptote quicker to the swarm settling velocity (Figure 7). The velocity as a function of time was determined from image analysis of the data set and represents the velocity of the leading edge of the swarm. Figure 7 shows that the 25 micron bead swarms asymptote quickly (in 2-3 seconds) to settling velocities of 0.62 mm/s for the 5 mm and 10 mm fracture apertures, respectively, and 1 mm/s for the 50 mm aperture fracture. The swarm settling velocity for the 5 mm and 10 mm case is only slightly greater than the settling velocity for a single 25 micron particle (0.54 mm/s). Also, the initial swarm velocity is on the order of 50 mm/s or roughly a factor of 4.2 times greater than that of the simulations. The factor 4.2 corresponds to a swarm composed of roughly 1670 particles, based on the equation from Nitsche & Batchelor [16] for swarms in unconfined fluids (i.e., no walls). From mass measurements, we estimate that our swarms were composed of roughly 1% solids by mass or roughly 7200 particles (or a factor of 18). We hypothesize that the release of the swarm above the air-water interface results in dissipation of energy and results in initially slower swarm velocities and the quick relaxation to a settling velocity.

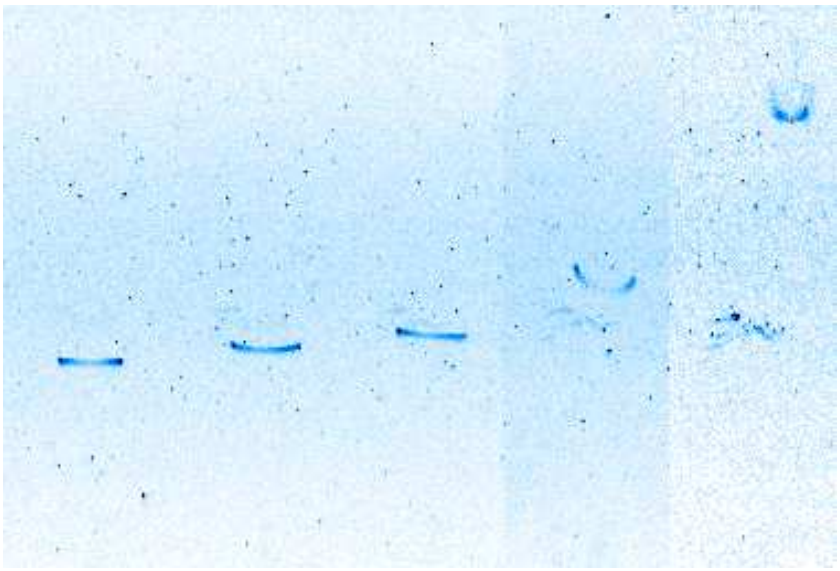

FIG. 6. *Composite images from 5 separate experiments showing the effect of smooth-walled uniform aperture fractures of 50 mm, 25 mm, 20 mm, 10 mm and 5 mm (from left to right) on swarms composed of 25 micron glass beads falling in water after an elapsed time of 11.16 seconds.*

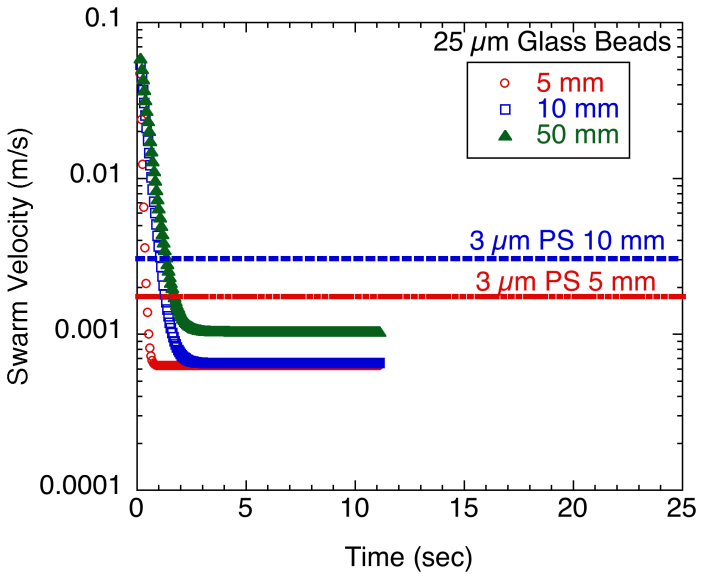

FIG. 7. *Swarm velocity as a function of time for swarms composed of 25 micron glass beads and swarms composed of 3 micron polystyrene beads.*

To examine this effect, we repeated the experiments using swarms composed of 3 micron diameter beads that were released in the water. For a single 3 micron particle, the settling velocity based on equation 1.1 is 2.7e-04 mm/s and should result in an initial swarm velocity of 18 mm/s based on the approximation of Nitsche & Batchelor [16] if not constrained by walls. We observed that the 3 micron particle swarms fell with a constant velocity for the 5 mm and 10 mm aperture fractures but with significantly lower velocities (1.7 mm/s and 3 mm/s, respectively) than the approximated values. However, the velocity remained constant as the swarms fell through the entire length of

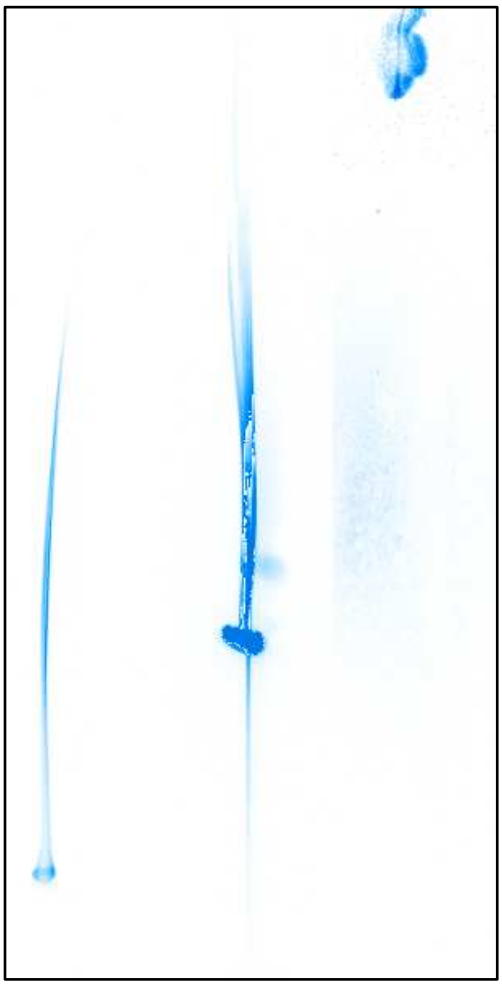

FIG. 8. *Composite image form 3 separate experiments for swarms composed of 3 micron beads released in water-filled smooth-walled fractures with aperture of 10 mm, 5 mm and 1mm (from left to right) for an elapsed time of 11.5 seconds*

the sample (100 mm). For the 1 mm aperture case, the particle interactions with the wall were significant (Figure 8) and took more than 27 minutes to fall 2/3 of the entire length of the sample.

6. Conclusions. Maintaining a collection of particles as they are transported through a fracture or fracture network has applications to targeted remediation with nano-particles or microbial communities as well as future potential for nano-sensor distribution. From our experiments and numerical simulations, we find that maintaining a particle swarm as it falls under gravity in a smooth-walled fracture is affected strongly by the walls of a fractures as well as interparticle spacing. In our experiments, dense swarms maintained a distinct cohesive body as they fell through the water but had significant particle leakage that formed a tail to the swarm. Interestingly, the tail of the swarm followed the same path as the initial swarm. Thus, in terms of targeting swarms of sensors to a given location, the particles in the tail of the swarm will flow to the same location as the main swarm body.

The decrease in velocity with decrease in fracture apertures presents a challenge for getting a collection of sensors deep into a fracture network in a significantly short time. We have begun preliminary numerical simulations and experimental design to examine the effect of a free stream

velocity on swarm cohesiveness.

7. Acknowledgments. The authors wish to acknowledge support of this work by the Geosciences Research Program, Office of Basic Energy Sciences US Department of Energy (DE-FG02-09ER16022) and the Summer Undergraduate Research Fellowship (SURF) program at Purdue University supported by Intel, the School of Science at Purdue and the Department of Physics.

References.

1. US Deparment of Energy, O.B.E.S., *Basic Research Needs in Geosciences: Facilitating 21st Century Energy Systems, Report from the Workshop held February 21-23*, 2007. 2007: Bethesda, MD. p. 262.
2. Sun, H., A.M. Scharff-Poulsen, H. Gu, and K. Almdal, *Synthesis and characterization of ratiometric, pH sensing nanoparticles with covalently attached fluorescent dyes.* Chemistry Of Materials, 2006. 18(15): p. 3381-3384.
3. Ma, A. and Z. Rosenzweig, *Synthesis and anlytical propertie of micrometric biosensing lipobeads.* Anal. Bioanal. Che, 2005. 382: p. 28-36.
4. Sun, H.H., A.M. Scharff-Poulsen, H. Gu, I. Jakobsen, J.M. Kossmann, W.B. Frommer, and K. Almdal, *Phosphate sensing by fluorescent reporter proteins embedded in polyacrylamide nanoparticles.* Acs Nano, 2008. 2(1): p. 19-24.
5. Poulsen, A.K., A.M. Scharff-Poulsen, and L.F. Olsen, *Horseradish peroxidase embedded in polyacrylamide nanoparticles enables optical detection of reactive oxygen species.* Analytical Biochemistry, 2007. 366(1): p. 29-36.
6. Anker, J.N., Y.E. Koo, and R. Kopelman, *Magnetically controlled sensor swarms.* Sensors And Actuators B-Chemical, 2007. 121(1): p. 83-92.
7. Anker, J.N., C.J. Behrend, H.M. Huang, and R. Kopelman, *Magnetically-modulated optical nanoprobes (MagMOONs) and systems.* Journal Of Magnetism And Magnetic Materials, 2005. 293(1): p. 655-662.
8. Jung, C.Y., H.S. Kim, H.Y. Kim, H.J. Ha, and S.M. Koo, *Multifunctional Hybrid Silica Partilces for Multicolor Imaging and Multiplex Tasking.* Nature Precedings, 2008. hdl:10101/npre.2008.1621.1: Posted 22 Feb 2008.
9. Kim, J.-I., Z. Ding, S.-N. Lee, J.-G. Yook, B. Ziaie, and D. Peroulis. *Hydrogel-Based Intergrated Antenna-pH Sensor.* in IEEE Sensors 2007 Conference. 2007: IEEE.
10. Lei, M., A. Baldi, E. Nuxoll, R.A. Siegel, and B. Ziaie, *A Hydrogel-Based Implantable Micromachined Transponder for Wireless Glucose Measurement.* Diabetes Technology and Therapeutics, 2006. 8: p. 112-122.
11. Sailor, M.J. and J.R. Link, *"Smart Dust": Nanostructured devices in a grain of sand.* Chemical Communications, 2005: p. 1375-1383.
12. Usami, M., A. Sato, H. Tanabe, T. Iwamatsu, S. Maegawa, and Y. Ohji. *An SOI0Based 7.5 μm-Thick 0.15 x 0.15 mm^2 RFID Chip. in IEEE International Solid-State Circuits Conference.* 1006: IEEE.
13. Yawazawa, Y., T. Oonishi, K. Watanabe, R. Nemoto, M. Kamahori, T. Hasebe, and Y. Akamatsu. *A Wireless Biosensing Chip for DNA Detection.* in IEEE International Solid-State Circuits Conference. 2005: IEEE.
14. Adachi, K., S. Kiriyama, and N. Yoshioka, *Behavior Of A Swarm Of Particles Moving In A Viscous-Fluid.* Chemical Engineering Science, 1978. 33(1): p. 115-121.
15. Ryan, J.N. and M. Elimelech, *Colloid mobilization and transport in groundwater.* Colloids And Surfaces A-Physicochemical And Engineering Aspects, 1996. 107: p. 1-56.
16. Nitsche, J. M. and G. K. Batchelor, *Break-up of a Falling Drop containing Dispersed Particles*, J. Fluid Mech., v.340, pp.161-175.
17. Machu, G., W. Meile, L.C. Nitsche, and U. Schaflinger, *Coalescence, torus formation and breakup of sedimenting drops: experiments and computer simulations.* Journal Of Fluid Mechanics, 2001. 447: p. 299-336.
18. Metzger, B., M. Nicolas, and E. Guazzelli, *Falling clouds of particles in viscous fluids.*

Journal Of Fluid Mechanics, 2007. 580: p. 283-301.
19. Machu, G., W. Meile, L. Nitsche, and U. Schaflinger, *The motion of a swarm of particles travelling through a quiescent, viscous fluid*. Zeitschrift Fur Angewandte Mathematik Und Mechanik, 2001. 81: p. S547-S548.
20. Ekiel-Jezewska, M.L., B. Metzger, and E. Guazzelli, *Spherical cloud of point particles falling in a viscous fluid*. Physics Of Fluids, 2006. 18(3).
21. Al Taweel, A.M., J. Militzer, J.M. Kan, and F. Hamdullahpur, *Motion Of Hydrodynamic Aggregates*. Powder Technology, 1989. 59(3): p. 173-181.
22. Faxen, von H., *The Resistance against the Movement of a rigour sphere in viscuous fluids which is embed between two parallel layered barriers*, Annalen der Physik, v.68, no 10, 1922.
23. Brenner, H., *The slow motion of a sphere through a viscous fluid towards a plane surface*, Chemical Engineering Science, v16, 242-251, 1961.
24. Grasselli, Y. and L. Lobry, *Hydrodynamic interactions between a particle and two rigid walls: Effect of surface roughness and many-body hydrodynamic interactions*, Phys. Fluids 9 (12), 3929-3931, December 1997